Molecular Cell, Volume *81*

Supplemental information

The Rad51 paralog complex Rad55-Rad57 acts as a molecular chaperone during homologous recombination

Upasana Roy, Youngho Kwon, Lea Marie, Lorraine Symington, Patrick Sung, Michael Lisby, and Eric C. Greene

SUPPLEMENTAL INFORMATION

Figure S1

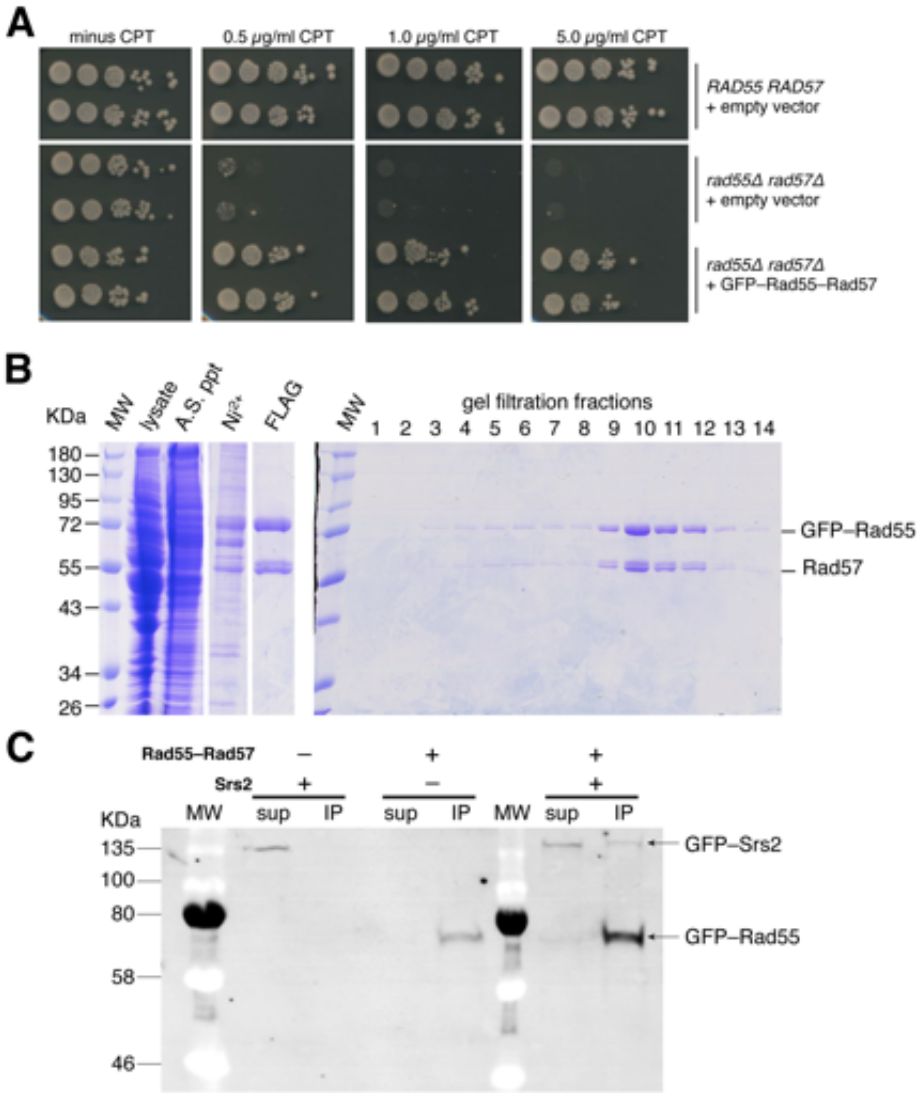

Figure S1. Preparation of the GFP–Rad55–Rad57 complex, related to Figure 1. (**A**) *RAD55 RAD57* cells were complemented with empty vector and *rad55Δ rad57Δ* cells were either complemented with empty vector, or a plasmid expressing GFP–tagged Rad55–Rad57. Colony growth of 2 separate clones was measured at the indicated concentrations of camptothecin (CPT). (**B**) Cell lysate, resuspended ammonium sulphate precipitate (A.S. ppt), elution from Ni^{2+} column, elution from FLAG column and fractions from the gel filtration column (0.5 mL fractions) were loaded on a 10% SDS PAGE gel and stained with Coomassie blue. (**C**) Pull–down with FLAG–Rad57 showing interaction of Rad55–Rad57 with GFP–Srs2. The supernatant (Sup) or bound (IP) fraction was blotted with anti–His antibody.

Figure S2

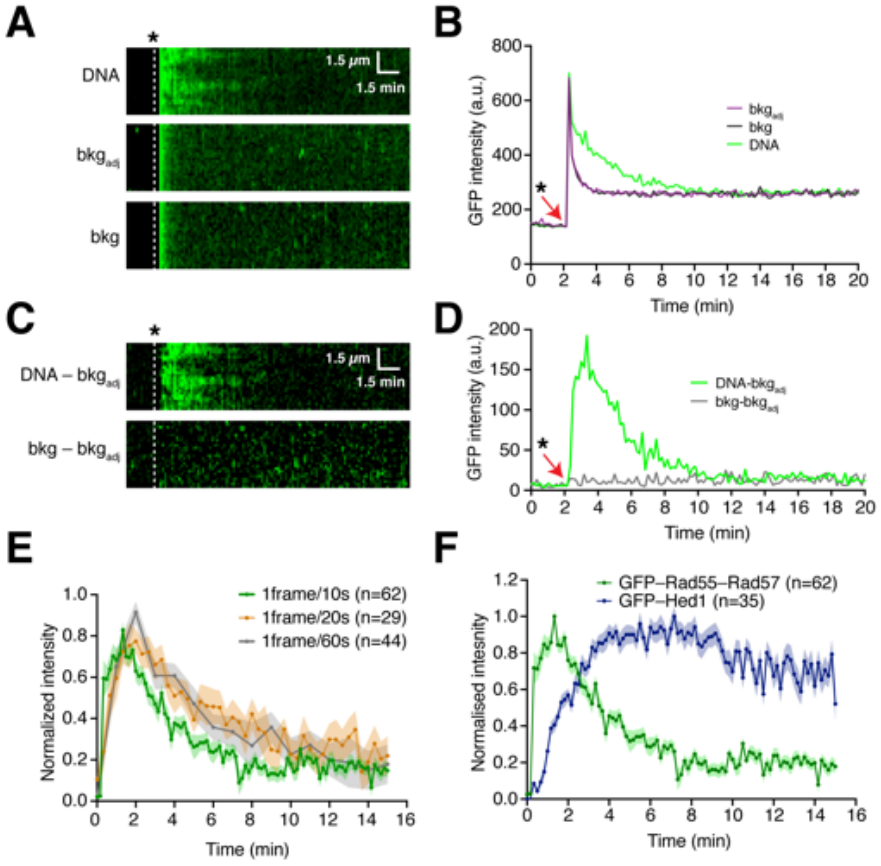

Figure S2. Rad55–Rad57 is depleted from mature Rad51 filaments, related to Figure 2. (**A**) Kymograph of GFP signal on a ssDNA molecule (DNA), background region adjacent to the ssDNA (bkg_{adj}) or a distal background region away from the DNA (bkg) during co–injection of 2 μM Rad51 and 60 nM GFP–Rad55– Rad57. (**B**) Integrated GFP intensity from kymographs in (A). The time of injection of Rad51 and GFP–Rad55–Rad57 is depicted by the white dashed line or red arrow. (**C**) Resultant images after background subtraction, and (**D**) the corresponding quantification. (**E–F**) Photobleaching controls to confirm transient binding of Rad55–Rad57 during Rad51–ssDNA filament formation. Data were derived using one to three flowcells per reaction condition. (**E**) Graph showing kinetics of Rad55–Rad57 after co–injection with Rad51 at varying laser exposure times. Normalized intensity is plotted for Rad55–Rad57 imaged at a rate of one frame per 10 s, 20 s or 60 s, as indicated; note, samples are only exposed to laser light during frame acquisition. Shaded areas represent 95% CI. (**F**) Comparison of the transient binding of GFP–Rad55–57 to the stable binding of GFP–Hed1 during Rad51–ssDNA filament formation; Hed1 is a meiosis–specific protein that binds tightly to Rad51 (Brown and Bishop, 2014; Crickard et al., 2018). Normalized intensity is plotted and the shaded area represents 95% CI.

Figure S3

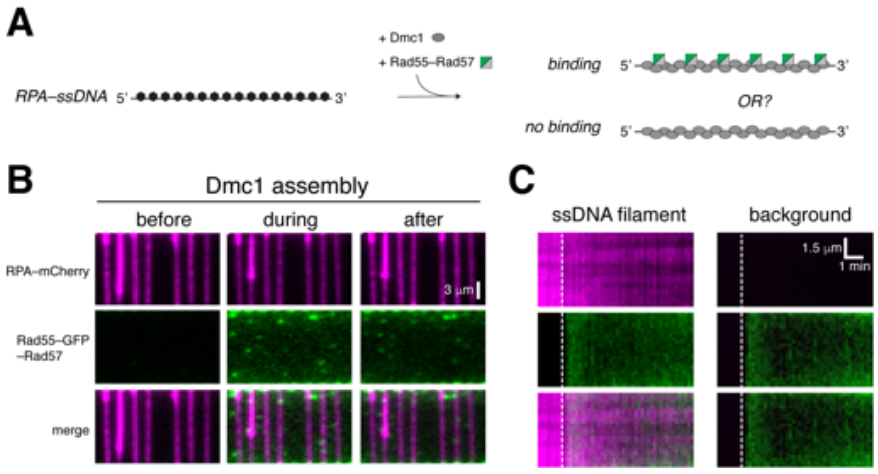

Figure S3. Rad55–Rad57 doesn't bind Dmc1–ssDNA filaments, related to Figure 2. (**A**) Assay schematic to test Rad55–57 binding during Dmc1–ssDNA filament assembly. (**B**) Wide–field view of RPA–mCherry bound ssDNA (magenta) 1 min before, during, and 1 min after co–injection of 60 nM Rad55–Rad57 (green) and 2 μM Dmc1. (**C**) Representative kymographs of Dmc1–ssDNA, and background region lacking ssDNA. Injection of GFP–Rad55–Rad57 is indicated by the white dashed line.

Figure S4

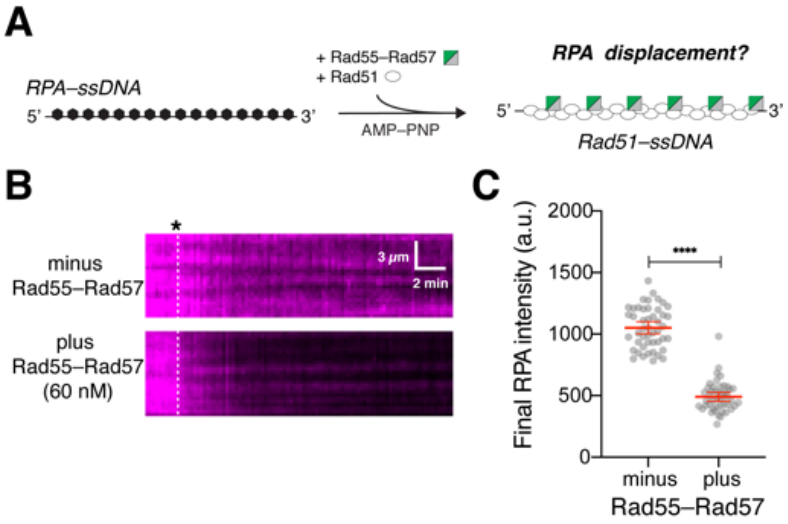

Figure S4. Rad55–Rad57 can promote RPA clearing by Rad51 in the presence of AMP–PNP, related to Figure 4. (**A**) Schematic for the experimental setup. (**B**) Kymographs of single representative DNA molecules showing loss of RPA–mCherry after Rad51 injection with 0 or 60 nM GFP–Rad55–Rad57 in the presence of AMP–PNP. Time of injection is indicated by a white dashed line. (**C**) RPA–mCherry signal remaining on the ssDNA molecules after Rad51 assembly plateaued in the presence of AMP–PNP, without (N = 47) or with 60 nM Rad55–Rad57 (N = 46). Red bars indicate mean ± 95% CI. Data were derived using two flowcells per reaction condition.

Figure S5

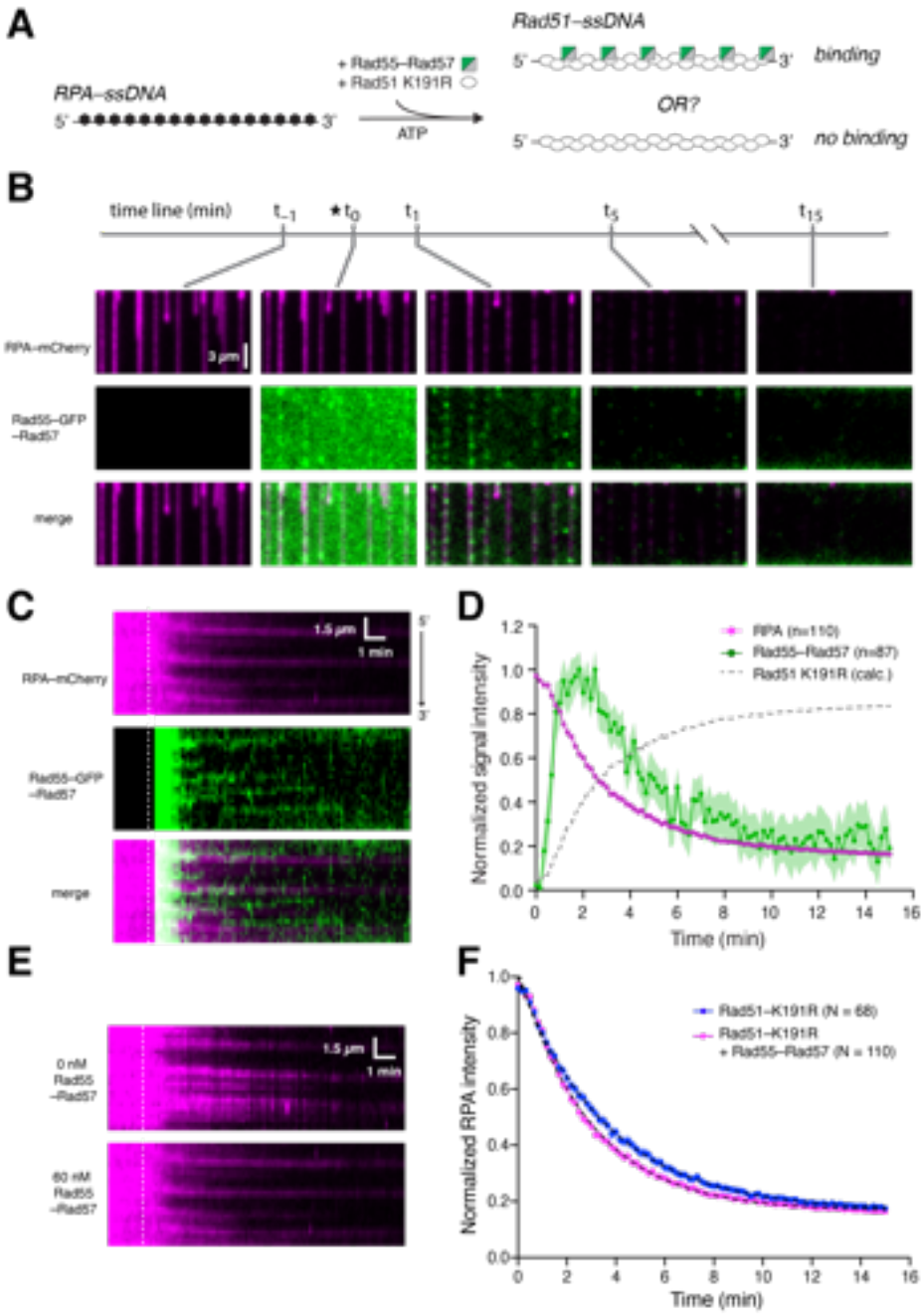

Figure S5. ATP hydrolysis by Rad51 is not required for binding and dissociation of Rad55–Rad57, related to Figure 4. (A) Experimental schematic for assays with Rad51–K191R. **(B)** Wide–field view of RPA– mCherry (magenta) bound ssDNA at the indicated time points. Time at which Rad51–K191R and Rad55–Rad57 (green) were co–injected is indicated with an asterisk (*). **(C)** Representative kymographs showing the behavior of mCherry–RPA and GFP–Rad55–Rad57.

(D) Graph showing the mean normalized signal intensities for RPA–mCherry and GFP–Rad55–Rad57. The shaded area represents the 95% CI. Data were derived using three flowcells. Calculated Rad51–K191R binding is plotted as [1–RPA] signal for comparison. **(E)** Representative kymographs showing RPA–mCherry loss at the indicated concentrations of Rad55–Rad57 co–injected with Rad51–K191R. **(F)** Graph showing kinetics of RPA in the presence of Rad51–K191R and either, 0 nM (blue), or 60 nM Rad55–Rad57 (magenta). Data were derived using three flowcells per reaction condition. It should be noted that due to its reduced ssDNA affinity, we could not use lower concentrations of Rad51–K191R at which any effect of Rad55–Rad57 would be apparent. Here we use 5 μM Rad51–K191R (compared to 2 μM WT Rad51) to allow for sufficient filament assembly (Kaniecki et al., 2017).

Figure S6

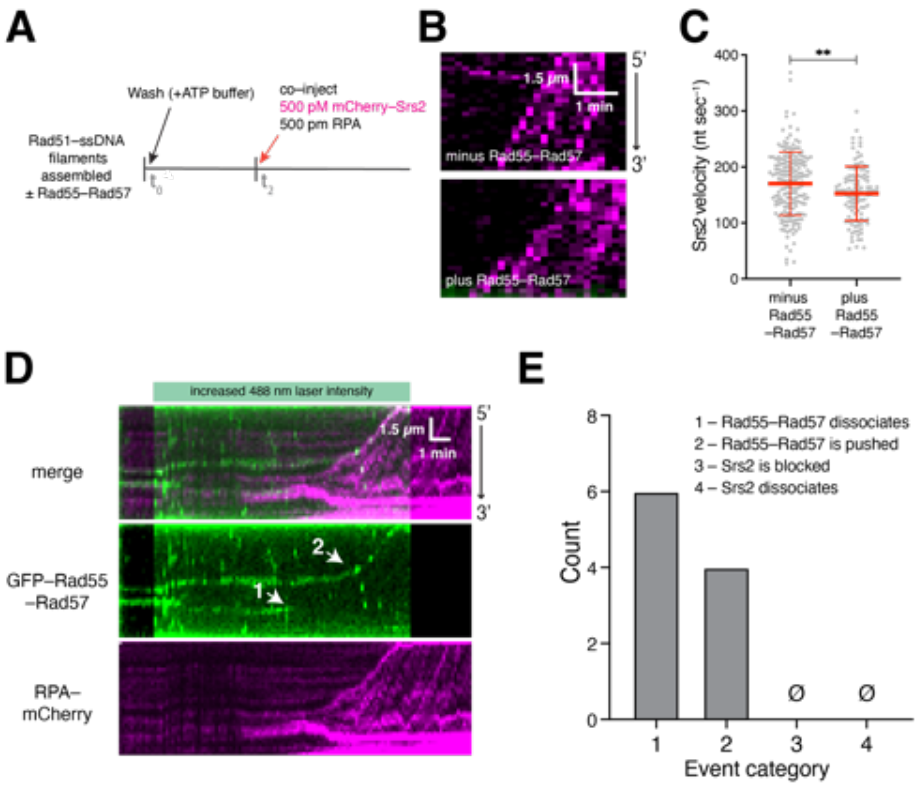

Figure S6. Srs2 strips residual Rad55–Rad57 from Rad51–ssDNA, related to Figure 6. (A) Assay schematic. **(B)** Kymographs showing mCherry–Srs2 (magenta) translocating on Rad51–ssDNA filaments formed in the absence (top) or presence (bottom) of Rad55–Rad57. **(C)** Quantification of Srs2 velocities in experiment (B). Data were derived using three flowcells per reaction condition. **(D)** Kymograph showing residual Rad55–57 foci (green) on Rad51–ssDNA and rebinding of RPA–mCherry (magenta) behind Srs2. Translocating Srs2 stripped off Rad55–Rad57 foci (1) or pushed it along the ssDNA in a 3'→5' direction (2, indicated by white arrows). **(E)** Quantification of observed outcomes when Srs2 encountered Rad55–Rad57 foci on DNA. Data were derived from two flowcells.

Figure S7

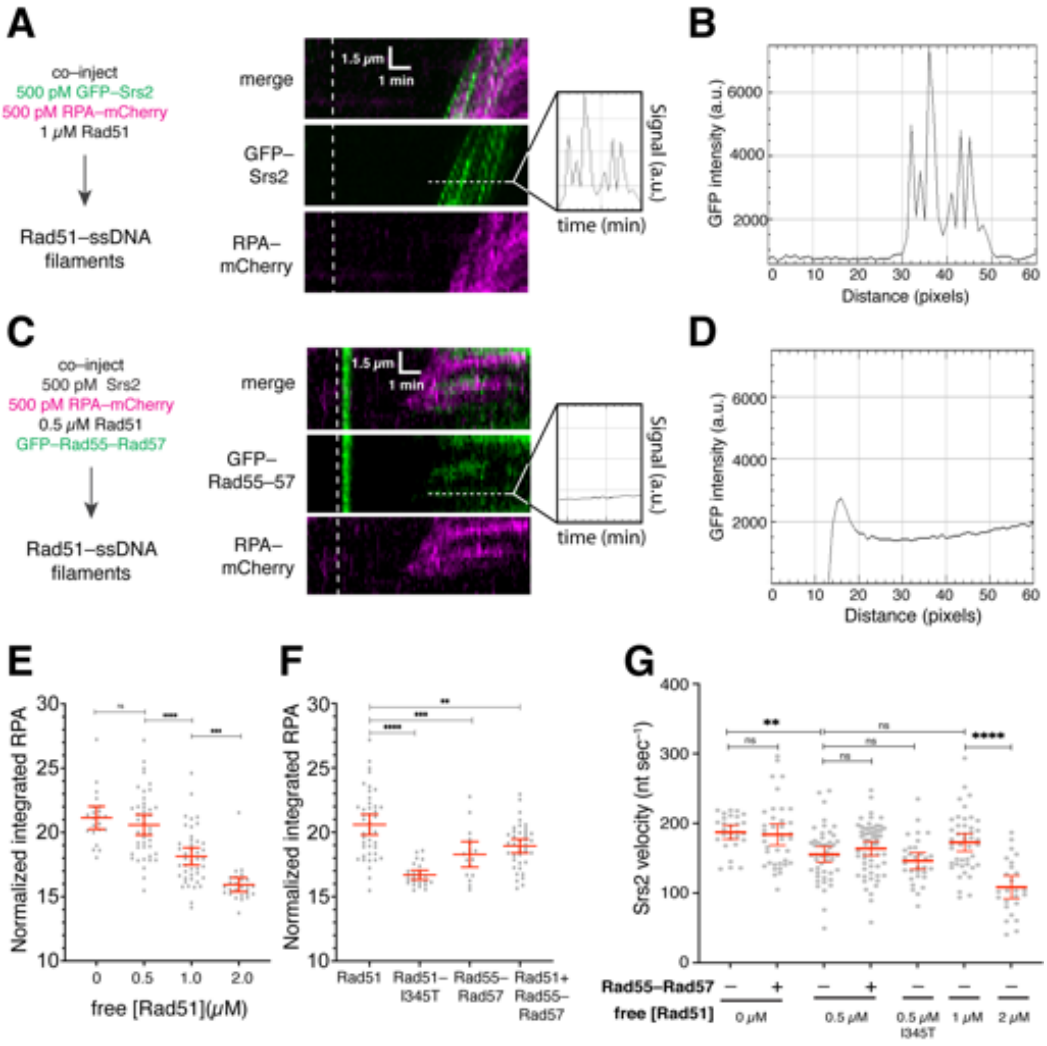

Figure S7. Quantification of GFP–Srs2 activity in the presence of free Rad51, RPA and Rad55–Rad57, related to Figure 6. (A) Assay schematic and example kymographs for the quantification of Srs2 activity on Rad51–ssDNA filaments. Time of protein co-injection is indicated with a white dashed line. Quantifications were done over a 2.5 min time window (as indicated) starting from the first Srs2 molecule translocation on Rad51–ssDNA filaments. Number of Srs2 molecules per Rad51– ssDNA filament was determined by number of peaks in the GFP intensity profile from individual kymographs (**B**) GFP intensity profile for kymograph in (A). (**C**) Assay schematic and example kymograph for control experiment with unlabeled Srs2 and GFP–Rad55–Rad57. Time of protein co-injection is indicated with a white dashed line (**D**) GFP intensity profile for kymograph in (C). (**E**) Quantification of RPA–mCherry rebinding after Srs2 translocation in the presence of either 0 μM Rad51 (N=22), 0.5 μM Rad51 (N=43), 1 μM Rad51 (N=43), or 2 μM Rad51 (N=26), expressed as normalized integrated mCherry signal intensity. Data were derived using at least two flowcells per reaction condition. (**F**) Quantification of RPA–

mCherry rebinding after Srs2 translocation in the presence of either 0.5 μM Rad51 (N=43, same as in (E)), 0.5 μM Rad51–I345T (N=24), 60 nM Rad55–Rad57 (N=17), or 0.5 μM Rad51 + 60 nM Rad55–Rad57 (N=40), expressed as normalized integrated mCherry signal intensity. Red bars indicate mean ± 95% CI. Data were derived using at least two flowcells per reaction condition. Quantifications in (E,F) were done over a 2.5 min time window starting from the first Srs2 molecule translocation on Rad51–ssDNA filament. **(G)** Quantification of Srs2 velocities with 0.5 nM free RPA–mCherry, ± 60 nM Rad55–Rad57 and 0–2 μM Rad51 or 0.5 μM Rad51–I345T, as indicated. The red lines indicate the means ± 95% CI for each data set. Data were derived using at least two flowcells per reaction condition.

Table S1. Rad51 filament assembly parameters, related to Figures 2, 3, 4 & S5.

	Filament assembly conditions	Fluorescence signal	Dissociation rate	95% CI	N	Fig.
			k (min^{-1})			
1	2 μM Rad51 + 2 mM ATP	RPA–mCherry	0.187	0.181 – 0.193	72	3C
2	2 μM Rad51 + 5 nM Rad55–Rad57 + 2 mM ATP	RPA–mCherry	0.355	0.351 – 0.359	90	3C
3	2 μM Rad51 + 60 nM Rad55–Rad57 + 2 mM ATP	RPA–mCherry	0.493	0.485 – 0.501	59	3C, 2D
		GFP–Rad55–Rad57	0.455	0.423 – 0.488	62	2D
4	2 μM Rad51 + 2 mM AMP–PNP	RPA–mCherry	0.129	0.119 – 0.140	80	4F
5	2 μM Rad51 + 60 nM Rad55–Rad57 + 2 mM AMP–PNP	RPA–mCherry	0.252	0.239 – 0.265	102	4D, 4F
		GFP–Rad55–Rad57	0.020		104	4D
6	5 μM Rad51–K191R + 2 mM ATP	RPA–mCherry	0.275	0.270 – 0.281	68	S5F
7	5 μM Rad51–K191R + 60 nM Rad55–Rad57 + 2 mM ATP	RPA–mCherry	0.339	0.334 – 0.344	110	S5D,F
		GFP–Rad55–Rad57	0.348	0.305 – 0.393	87	S5D

Table S2. Srs2 translocation parameters, related to Figures 6, S6 & S7.

	Reaction description	Srs2 co–injected with	Srs2 velocity (nt sec^{-1})			No. of Srs2 molecules			Fig.
			mean	s.d.	N	mean	s.d.	N	
1	500 pM GFP–Srs2 on pre–assembled Rad51 filaments	500 pM RPA–mCherry	175.3	±33.2	55	6.6	±1.4	47	6B,C, S7G
2	500 pM GFP–Srs2 on pre–assembled Rad51 filaments	500 pM RPA–mCherry	163.6	±48.8	65	6.5	±1.2	64	6E,F, S7G
		60 nM GFP–Rad55–Rad57							
3	500 pM GFP–Srs2 on pre–assembledRad51 filaments	500 pm RPA–mCherry	156.2	±36.8	59	6.4	±1.4	61	6B–F, S7G
		0.5 μM Rad51							
4	500 pM GFP–Srs2 on pre–assembledRad51 filaments	500 pM RPA–mCherry	169.2	±41.6	44	3.9	±1.7	34	6B,C, S7G
		1 μM Rad51							
5	500 pM GFP–Srs2 on pre–assembledRad51 filaments	500 pM RPA–mCherry	105.1	±39.8	25	2.5	±1.5	26	6B,C, S7G
		2 μM Rad51							
6	500 pM GFP–Srs2 on pre–assembledRad51 filaments	500 pM RPA–mCherry	153.9	±35.61	63	4.5	±1.8	68	6E,F, S7G
		0.5 μM Rad51							
		60 nM Rad55–Rad57							
7	500 pM GFP–Srs2 on pre–assembled Rad51 filaments	500 pM RPA–mCherry	142.7	±32.61	31	4.9	±1.7	36	6E,F, S7G
		0.5 μM Rad51–I345T							
8	500 pM mCherry–Srs2 on pre–assembled Rad51 filaments	500 pM unlabeled RPA	170	±56.5	194	n.a.			S6B,C
9	500 pM mCherry–Srs2 on Rad51 filaments pre–assembled with 60 nM Rad55–Rad57	500 pM unlabeled RPA	152	±48.5	119	n.a.			S6B,C